nature physics

ARTICLES

PUBLISHED ONLINE: 21 SEPTEMBER 2015 | DOI: 10.1038/NPHYS3471

A density-independent rigidity transition in biological tissues

Dapeng Bi[1], J. H. Lopez[1], J. M. Schwarz[1,2] and M. Lisa Manning[1,2]*

Cell migration is important in many biological processes, including embryonic development, cancer metastasis and wound healing. In these tissues, a cell's motion is often strongly constrained by its neighbours, leading to glassy dynamics. Although self-propelled particle models exhibit a density-driven glass transition, this does not explain liquid-to-solid transitions in confluent tissues, where there are no gaps between cells and therefore the density is constant. Here we demonstrate the existence of a new type of rigidity transition that occurs in the well-studied vertex model for confluent tissue monolayers at constant density. We find that the onset of rigidity is governed by a model parameter that encodes single-cell properties such as cell–cell adhesion and cortical tension, providing an explanation for liquid-to-solid transitions in confluent tissues and making testable predictions about how these transitions differ from those in particulate matter.

Important biological processes such as embryogenesis, tumorigenesis and wound healing require cells to move collectively within a tissue. Recent experiments suggest that when cells are packed ever more densely, they start to exhibit collective motion[1–3] traditionally seen in non-living disordered systems such as colloids, granular matter, or foams[4–6].

Collective behaviours in these non-living systems are governed by a 'jamming' transition from a fluid-like state to a solid-like state that occurs as the density approaches a critical packing density of particles ϕ_c (ref. 6). This is also called a rigidity transition, because the material becomes linearly stable with respect to infinitesimal perturbations and begins to support shear stresses. Many of these effects are also seen in self-propelled particle (SPP) models[7]. In SPP models, overdamped particles experience an active force that causes them to move at a constant speed, and particles change direction owing to interactions with their neighbours or an external bath. To model cells with a cortical network of actomyosin and adhesive molecules on their surfaces, particles interact as simple repulsive disks or spheres, sometimes with an additional short-range attraction[8,9]. These models also exhibit a rigidity/jamming transition at $\phi_c < 1$ (refs 1,8,10,11), and near the transition point they exhibit collective motion[8] that is very similar to that seen in experiments[12].

An important open question is whether the density-driven rigidity transition in SPP models explains the collective behaviour observed in non-proliferating confluent biological tissues, where there are no gaps between cells and the packing fraction ϕ is fixed at precisely unity. For example, zebrafish embryonic explants are confluent three-dimensional tissues where the cells divide slowly—and therefore the number of cells per unit volume remains nearly constant. Nevertheless, these tissues exhibit hallmarks of glassy dynamics, such as caging behaviour and viscoelasticity. Furthermore, ectoderm tissues have longer relaxation timescales than mesendoderm tissues, suggesting ectoderm tissues are closer to a glass transition, despite the fact that both tissue types have the same density[1]. This indicates that there should be an additional parameter controlling the mechanical response in confluent tissues.

In this work, we study confluent monolayers using the vertex model[13–22], to determine how tissue mechanical response varies with single-cell properties such as adhesion and cortical tension. We find a new type of rigidity transition that is not controlled by the density, but instead by a dimensionless target shape index that is specified by single-cell properties. This rigidity transition possesses several hallmarks of a second-order phase transition. These findings provide a novel explanation for liquid-to-solid transitions in tissues that remain at constant density.

The vertex model, which agrees remarkably well with experimental data for confluent monolayers[13–21], approximates the monolayer as a collection of adjacent columnar cells. The mechanical energy of a single cell labelled 'i' is given by[14,16]:

$$E_i = K_{A_i}(A_i - A_{i0})^2 + \xi_i P_i^2 + \gamma_i P_i \tag{1}$$

The first term results from a combination of three-dimensional cell incompressibility and the monolayer's resistance to height fluctuations or cell bulk elasticity[15,23]. Then K_{A_i} is a height elasticity, and A_i and A_{i0} are the actual and preferred cell cross-sectional areas.

The second term in equation (1) is quadratic in the cell cross-sectional perimeter P_i and models the active contractility of the actin–myosin subcellular cortex, with elastic constant ξ_i (ref. 14), and the last term represents an interfacial tension γ_i set by a competition between the cortical tension and the energy of cell–cell adhesion[18,24] between two contacting cells. γ_i can be positive if the cortical tension is greater than the adhesive energy, or negative if the adhesion dominates. It is also possible to incorporate strong feedback between adhesion and cortical tension in this term[18,25]. As only the effective forces—the derivatives of the energy with respect to the degrees of freedom—are physically relevant, equation (1) can be rewritten as $E_i = K_{A_i}(A_i - A_{i0})^2 + \xi_i(P_i - P_{i0})^2$, where $P_{i0} = -\gamma_i/(2\xi_i)$ is an effective target shape index.

As discussed in ref. 16, when all single-cell properties are equal ($K_{A_i} = K_A$, $\xi_i = \xi$, $A_{i0} = A_0$, $P_{i0} = P_0$), the total mechanical energy of a tissue containing N cells can be non-dimensionalized:

$$\varepsilon = \frac{1}{K_A A_0^2}\sum_{i=1}^{N} E_i = \sum_{i=1}^{N}\left[(\tilde{a}_i - 1)^2 + \frac{(\tilde{p}_i - p_0)^2}{r}\right] \tag{2}$$

where $\tilde{a}_i = A_i/A_0$ and $\tilde{p}_i = P_i/\sqrt{A_0}$ are the rescaled shape functions for area and perimeter. $r = K_A A_0/\xi$ is the inverse perimeter modulus

[1]Department of Physics, Syracuse University, Syracuse, New York 13244, USA. [2]Syracuse Biomaterials Institute, Syracuse, New York 13244, USA.
*e-mail: mmanning@syr.edu

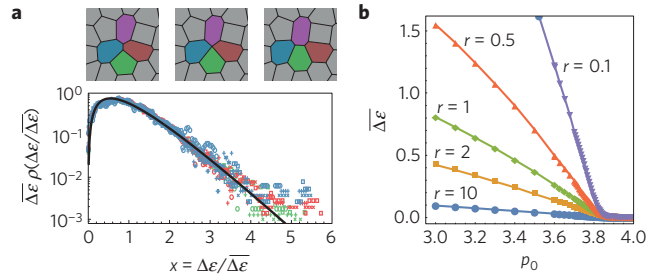

Figure 1 | Energy barriers for local cellular rearrangements. a, Illustration of a T1 transition in a confluent tissue and the normalized distribution ρ of normalized energy barrier heights $\Delta\varepsilon/\overline{\Delta\varepsilon}$ for a large range of parameters ($r=0.5, 1, 2$ and $p_0=3.2$–3.7). They have a universal shape that is fitted well by a k-gamma distribution (solid line), indicating that $\overline{\Delta\varepsilon}$ completely specifies the distribution and describes the mechanical response. **b**, $\overline{\Delta\varepsilon}$ as function of the target shape index p_0 for various values of the inverse perimeter modulus r.

and $p_0 = P_0/\sqrt{A_0}$ is the target shape index or a preferred perimeter-to-area ratio. For simplicity, we focus on $p_0 > 0$. For $p_0 < 0$ there are two regimes: a static regime with results identical to those presented here for $0 < p_0 < p_{\mathrm{pent}}$, and a coarsening regime that is not consistent with most observations of biological tissues. Geometrically, a regular hexagon corresponds to $p_0^{\mathrm{hex}} = 2\sqrt{2}\sqrt[4]{3} \approx 3.72$ and a regular pentagon to $p_0^{\mathrm{pent}} = 2\sqrt{5(5-2\sqrt{5})} \approx 3.81$.

In non-biological materials, bulk quantities such as shear/bulk modulus, shear viscosity and yield stress are often used to describe the mechanical response to external perturbations. However, cells are self-propelled and, even in the absence of external forces, cells in confluent tissues regularly intercalate, or exchange neighbours[26,27]. In an isotropic confluent tissue monolayer where mitosis (cell division) or apoptosis (cell death) are rare, cell neighbour exchange must happen through intercalation processes known as T1 transitions[28,29], where an edge between two cells shrinks to a point and a new edge arises between two neighbouring cells, as illustrated in Fig. 1a. The mechanical response of the tissue is governed by the rate of cell rearrangements, and, within the vertex model, the rate of T1 rearrangements is related to the amount of mechanical energy required to execute a T1 transition[29]. Therefore, we first study how these energy barriers change with single-cell properties encoded in the model parameters r and p_0.

To explore the statistics of energy barriers, we test all possible T1 transition paths (see Methods) in ten randomly generated disordered samples each consisting of $M = 64$ cells. For each value of p_0 and r tested, we obtained the distribution of energy barrier heights $\rho(\Delta\varepsilon)$. The functional form of the distribution becomes universal (Fig. 1a) when scaled by the mean energy barrier height $\overline{\Delta\varepsilon}(r, p_0)$. The rescaled distribution is fitted well by a k-gamma distribution $(k^k x^{k-1} \exp(-kx)/(k-1)!)$ with $x = \Delta\varepsilon/\overline{\Delta\varepsilon}$ and $k = 2.2 \pm 0.2$. The k-gamma distribution has been observed in many non-biological disordered systems[30–32], and generically results from maximizing the entropy subject to constraints[31,32]. This confirms that the distribution of energy barriers depends on the single-cell properties p_0 and r only through its average $\overline{\Delta\varepsilon}$.

Figure 1b shows the dependence of $\overline{\Delta\varepsilon}$ on p_0 for various values of r. At $p_0 \lesssim 3.8$, the energy barriers are always finite—that is, cells must put in some amount of work to deform and rearrange. Here the tissue behaves like a solid; it is a rigid material with a finite yield stress. As p_0 is increased, the energy barriers decrease and become vanishingly small in the vicinity of $p_0 \approx 3.8$, so that cell rearrangements cost almost no energy. This suggests that the vertex model may undergo a critical rigidity transition near $p_0 \approx 3.8$.

To test this hypothesis, we searched for a scaling collapse based on theories for continuous phase transitions near a critical point, such as the Ising model for ferromagnetism. Figure 1b demonstrates that r sets the overall scale of $\overline{\Delta\varepsilon}$ as well as the 'sharpness' of the transition, whereas p_0 controls the distance to the transition. This suggests that the trio $(r\overline{\Delta\varepsilon}, r, p_0 - p_0^*)$ is analogous to $(m, h, T - T_c)$ in the Ising model. Therefore, our scaling ansatz is that the order parameter $r\overline{\Delta\varepsilon}(r, p_0)$ vanishes at the critical point $p_0 = p_0^*$, with fluctuations controlled by r. In that case, near the critical point the order parameter should obey the universal scaling form[33]:

$$r\overline{\Delta\varepsilon} = |p_0 - p_0^*|^{\beta} f_{\pm}\left(\frac{r}{|p_0 - p_0^*|^{\Delta}}\right) \tag{3}$$

Here $z = r/|p_0 - p_0^*|^{\Delta}$ is the crossover scaling variable, Δ is the crossover scaling critical exponent, and f_-, f_+ are the two branches of the crossover scaling functions for $p_0 < p_0^*$ and $p_0 > p_0^*$, respectively.

After re-plotting the data in Fig. 1b using equation (3), we find an excellent scaling collapse onto two branches with $\Delta = 4.0 \pm 0.4$, $\beta = 1.0 \pm 0.2$ and a precise location of the critical point $p_0^* = 3.813 \pm 0.005$, as shown in Fig. 2.

For the mechanically rigid branch in the limit $z \to 0$, the energy barrier can be rewritten in dimensional units and scales as $\Delta E = K_A A_0^2 \overline{\Delta\varepsilon} \propto A_0 \xi \left(p_0^* - p_0\right)^{\beta}$. This indicates that these barriers are completely governed by the perimeter elasticity ξ. At the critical point, the two branches of the scaling function merge and $f_+ = f_- = z^{\beta/\Delta}$. In this case the dimensional energy barrier scales as

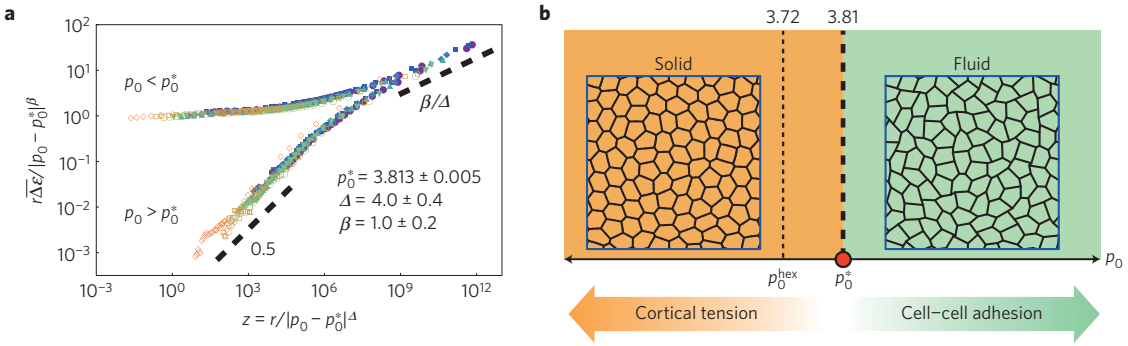

Figure 2 | A rigidity transition in confluent tissues. a, Critical scaling collapse of the average energy barrier height $\overline{\Delta\varepsilon}$, normalized by multiplying $r/|p_0 - p_0^*|^{\beta}$, as a function of $z = r/|p_0 - p_0^*|^{\Delta}$ for the data shown in Fig. 1b, confirming the scaling ansatz of equation (3). **b**, The rigidity transition is demonstrated in a simple phase diagram as a function of p_0, snapshots are taken from a typical rigid tissue ($p_0 = 3.7$) and fluid-like tissue ($p_0 = 3.96$). A rigidity transition occurs at $p_0 = p_0^* \approx 3.813$ for disordered metastable tissue configurations. The line corresponding to the order-to-disorder transition reported by Staple *et al.*[16] is shown for comparison. Below p_0^{hex}, the ground state is a hexagonal lattice, and above p_0^{hex}, the ground state is disordered.

$\Delta E = A_0^{2\beta/\Delta} K_A^{\beta/\Delta} \xi^{1-\beta/\Delta}$, which means the energy barriers vanish at the transition in the limit $K_A \to 0$ or $r \to 0$.

This scaling collapse is similar to those seen in jamming in particulate matter[4,34] and rigidity percolation on random networks[35–37], suggesting that p_0^* is a critical point analogous to Point J in the jamming transition or the critical occupation probability p^* in random network models. However, unlike the jamming transition, which is density driven, density can not control the rigidity transition in the vertex model because everything takes place at a packing fraction of unity. Instead, this model exhibits a novel rigidity transition controlled by the target shape index, p_0. Figure 2b summarizes these results in a simple phase diagram. Although we focus on the simple case where cells are identical, the rigidity transition is robust to small variations in cell properties (see Supplementary Section IV).

Although we calculate T1 transitions by shortening or lengthening a single cell–cell contact, our analysis of these local perturbations suggests a critical mechanical response with a growing length scale. To confirm and quantify these changes in the macroscopic mechanical response, we study the vibrational spectrum of the dynamical matrix[38,39]. We diagonalize the dynamical matrix to obtain normal modes and their corresponding eigenvalues $\{\lambda_i\}$ (Methods). If all the eigenvalues are positive (except for the trivial global translation modes with $\lambda = 0$), then the system is mechanically rigid, and we associate each positive eigenvalue with an eigenfrequency $\omega_i = \sqrt{\lambda_i}$ that describes the oscillations of each mode as the system is perturbed about its stable point. In contrast, non-trivial zero eigenvalues correspond to floppy eigenmodes—collective displacements of the vertices that cost zero energy—and if these exist then the system is a fluid.

We define the cumulative density of states using equation (4):

$$N(\omega) = \int_{0^+}^{\omega} D(\omega')\mathrm{d}\omega' + N(\lambda = 0)\,\theta(\omega) \tag{4}$$

where $D(\omega)$ is the density of vibrational states[38], $N(\lambda = 0)$ is the fraction of non-trivial zero eigenvalues, and $\theta(\omega)$ is the Heaviside step function.

In Fig. 3a,b we show the vibrational density of states obtained by averaging over 100 random samples each containing $M = 64$ cells. For $p_0 < p_0^*$, $N(\omega)$ exhibits Debye scaling $\omega^d = \omega^2$ (ref. 38) and approaches zero at zero frequency, which indicates that the tissue possesses a well-defined stable linear response and is therefore a solid. At $p_0 > p_0^* = 3.813$, Fig. 3a plateaus to a finite value as $\omega \to 0$, which indicates the emergence of floppy modes (that is, the existence of non-trivial zero eigenvalues). In addition, as the system approaches the rigidity transition from the solid phase, the density of states $D(\omega)$ exhibits a peak that shifts to lower frequencies (Fig. 3b), just as the so-called boson peak[39–41] in jammed particle packings and glasses. Interestingly, the shape and scaling of the peak is different from those in particulate matter, and this is an interesting avenue for future research.

Just as in jamming[42], the critical point at which the system becomes floppy fluctuates between different finite-size samples, as shown in Fig. 3c. Therefore, we define $p_{0\alpha}^*$ as the value of p_0 at which the number of non-trivial zero modes first becomes non-zero for a particular finite-size sample, labelled α, and perform finite-size scaling on the distributions of $p_{0\alpha}^*$ across many samples. In Supplementary Section I, we demonstrate that these distributions are independent of r, indicating that M alone controls the fluctuations. Figure 3d shows that the mean of the $p_{0\alpha}^*$ distribution approaches $p_0^* = 3.813$ in the limit of large system sizes, and the variance vanishes as $M^{-1/\nu}$, where $\nu \approx 1.33 \pm 0.05$ is obtained from a least-squares fit. This establishes that the rigidity transition takes place at the well-defined value of p_0^* in the thermodynamic limit.

Another standard measure of linear mechanical response is the shear modulus. We probe the tissue near the rigidity transition

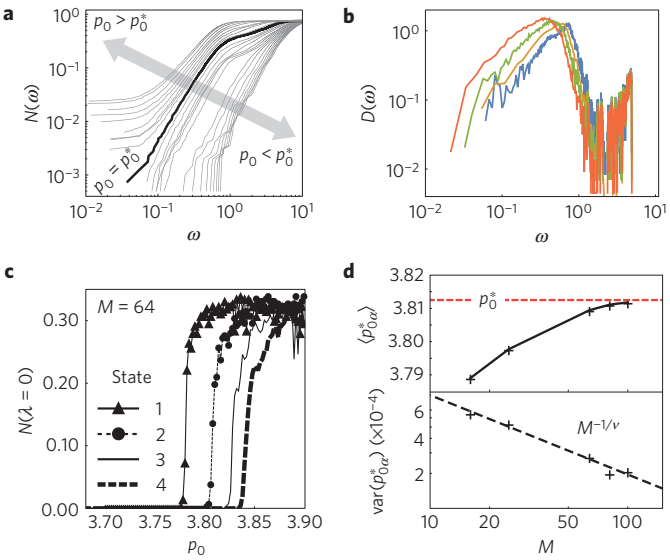

Figure 3 | Analysis of the vibrational density of states. a, The cumulative vibrational density of states $N(\omega)$ for $\omega \geq 0$ exhibits a rigidity transition at $r = 0.1$ and $p_0^* = 3.813$ (thick line). Thin lines correspond to $r = 0.1$ and values of p_0 ranging from 3.78 to 3.83 in increments of 10^{-3}. **b**, Vibrational density of states $D(\omega)$ for selected p_0 values, from left to right: 3.78, 3.79, 3.80, 3.81. At low ω, $D(\omega) \sim \omega$ follows Debye scaling before arriving at a boson peak. As p_0 is decreased towards the rigidity transition, the boson peak also shifts to lower frequencies. **c**, The fraction of non-trivial zero eigenvalues in the dynamical matrix $N(\lambda = 0)$ as a function of p_0 becomes finite at some $p_{0,\alpha}^*$, indicating the appearance of floppy modes or the loss of rigidity. Different lines correspond to four instances of this transition at system size $M = 64$ with different random initial conditions. **d**, For finite systems, the location of the rigidity transition $p_{0,\alpha}^*$ is distributed with a mean $\langle p_{0\alpha}^* \rangle$ that shifts as a function of system size M and approaches $p_0^* = 3.813$ as $M \to \infty$, and a variance that decays as $M^{-1/\nu}$ with an exponent $\nu \approx 1.33$.

in response to a quasistatic simple shear strain γ_{xy} and calculate the shear modulus G_{xy} (Methods). For systems with finite size, we plot the shear modulus as function of $p_{0\alpha}^* - p_0$. Figure 4 shows that the shear modulus vanishes as $G_{xy} \propto (p_{0\alpha}^* - p_0)/r$, which is yet another indication that this is a rigidity transition. In Supplementary Section III, we also analyse the behaviour of the shear modulus when averaged over $p_{0\alpha}^*$, which may be relevant for experimental measurements.

An obvious remaining question is what sets the critical point $p_0^* \sim 3.81$. To answer this question, we first study a simple mean-field model for a T1 topological swap. In an infinite confluent tissue, the topological Gauss–Bonnet theorem requires each cell to have six neighbours on average[28]. Therefore our mean-field model consists of four adjacent six-sided cells. To mimic the effect of additional neighbouring cells, we fix each cell area equal to unity. Equation (2) then becomes:

$$\varepsilon_4 = \sum_{4\ \text{cells}} (\tilde{p}_i - p_0)^2; \quad a_i = 1 \tag{5}$$

Equation (5) is calculated numerically during a T1 rearrangement (Methods), as shown in Fig. 5a. The total energy during this process is shown in Fig. 5b as the edge length ℓ is contracted (negative values) and a new edge is extended (positive values); the energy barrier $\Delta\varepsilon$ is the difference in energy between the initial and maximum energy state. As p_0 increases, $\Delta\varepsilon$ decreases as shown in Fig. 5c. The precise value p_0^* at which energy barriers vanish can be estimated by calculating the energy cost of shrinking an edge of length $\ell = \ell_0$ inside a hexagonal lattice, while all other edges remain unchanged. Precisely at the T1 transition, two of

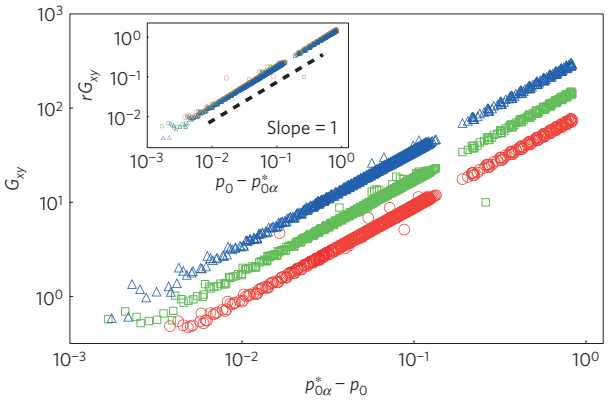

Figure 4 | Shear modulus as a function of $p^*_{0\alpha} - p_0$, which is the system-specific distance to the rigidity transition. The value of $p^*_{0\alpha}$ is determined from the location at which floppy modes appear for the specific configuration. Here the tissue contains $M = 100$ cells and the colours correspond to (top to bottom): $r = 0.005$ (blue), $r = 0.001$ (green) and $r = 0.02$ (red). Inset: the shear modulus can be rescaled by $G_{xy} = (p^*_{0\alpha} - p_0)/r$. Data for ten tissues with random initial configurations are shown.

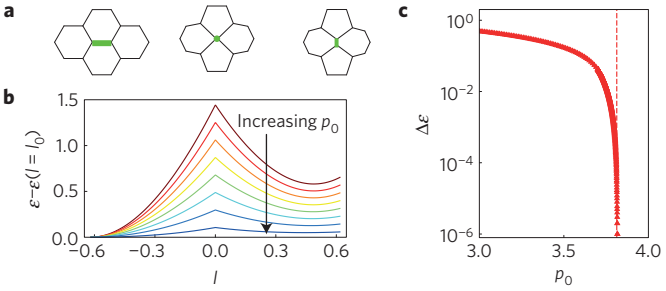

Figure 5 | A simple four-cell model. a, A four-cell aggregate undergoing a T1 topological swap. The thick (green) edge represents the cell–cell interface that is contracted to a point and then resolved in the perpendicular direction. **b**, Energy of a four-cell aggregate during a T1 transition, which attains a maximum at the transition point. p_0 varies from 1.5 to 3.8 in equal increments. **c**, Energy barrier height as a function of p_0 for a four-cell aggregate and a mean-field estimate (dashed) for the value of $p_0 = p_0^{\mathrm{pent}}$ at which $\Delta\varepsilon$ vanishes.

the cells are pentagons, whereas the other two remain hexagonal. Therefore if $p_0 < p_0^{\mathrm{pent}} = (7+2\sqrt{7})/(\sqrt{2}\times 3^{3/4}) \approx 3.812$, pentagons cost finite energy and therefore the transition necessarily requires finite energy. In contrast, for $p_0 \geq p_0^{\mathrm{pent}}$, pentagons (and n-gons with $n > 5$) cost no energy and the cells are able to remain in the ground state throughout the transition, requiring zero energy. The estimate $p_0^* = p_0^{\mathrm{pent}}$, indicated by a red dashed line in Fig. 5c, does identify the critical target shape index in our mean-field model, and is consistent with the critical point $p_0^* = 3.813 \pm 0.005$ identified by the scaling collapse of energy barriers in the full vertex model.

Is there an even simpler explanation for $p_0^* \sim p_0^{\mathrm{pent}}$? As in other rigidity transitions[6,35,36,40], we expect that the critical shape index should also be related to isostaticity. In the vertex model with periodic boundary conditions, cells tile the flat two-dimensional plane, and therefore the total number of vertices V, cells M and edges E are related through Euler's formula: $0 = V - E + M$. As each edge is shared by two cells, E is also related to the average coordination number z of cells or $E = Mz/2$, which yields $V = M(z/2 - 1)$. The degrees of freedom are simply the motions of each vertex in two dimensions: $n_{\mathrm{dof}} = 2V$. Assuming force balance (in both directions) and torque balance on each cell generates three constraints per cell: $n_c = 3M$. At isostaticity, the number of degrees of freedom equals the number of constraints: $n_{\mathrm{dof}} = n_c$, resulting in $z_{\mathrm{iso}} = 5$ and suggesting a mean-field transition at a shape index of $p_0^* \simeq 3.812$. Although it gives a correct prediction, this isostatic argument makes a strong assumption: that constraints are applied to each cell instead of to each vertex. Therefore, an interesting direction for future research is to understand under what circumstances the energy functional (equation (2)) effectively groups vertices into functional units that are cells.

Discussion

Although the vertex model has been used extensively to model tissues over the past 15 years, there has never been a clear way to connect the model parameters to tissue mechanical properties. Here we show that the vertex model has a new and previously unreported critical rigidity transition that occurs at a critical value of the target shape index $p_0^* \sim 3.81$. This criticality is evident in energy barriers to local T1 rearrangements, the vibrational spectrum of the linear response, and the shear modulus of the tissue. Unlike SPP models, where the liquid-to-solid transition is governed by density, our model has a constant-density glass transition governed by single-cell mechanical properties such as cell–cell adhesion and cortical tension encoded in the target shape index p_0.

Analysing only the ground states of the vertex model, the seminal work of Staple *et al.*[16] found an ordered-to-disordered transition at $p_0 = p_0^{\mathrm{hex}} \sim 3.722$. However, because almost all biological tissues are strongly disordered, it remained unclear whether this transition was relevant for the observed glass or jamming transitions in multicellular tissues. Therefore, we explicitly study disordered metastable states and transitions between them. In addition ref. 16 uses a linear stability analysis of a single cell to suggest that a rigidity transition also occurs at p_0^{hex}. In contrast, our analysis explicitly includes multicellular interactions (that is, collective normal modes) and nonlinear effects (that is, energy barriers). With this more sophisticated analysis, we demonstrate that vertex models exhibit a rigidity transition at a value $p_0 = p_0^{\mathrm{pent}} \sim 3.81$ that is measurably different from the prediction $p_0 = p_0^{\mathrm{hex}}$ based on single-cell linear stability.

Importantly, predictions based on this critical rigidity transition have recently been verified in experiments[43]. Specifically, in both simulations and experiments we can measure the shape index $p = P/\sqrt{A}$ for each cell in a monolayer, where P is the projected cell perimeter and A is the cross-sectional area. In simulations of the vertex model, we find that the median value of the observed shape index $\bar{p}$ is an order parameter that also exhibits critical scaling: $\bar{p} = p_0^* \sim 3.81$ for rigid or jammed tissues and $\bar{p}$ becomes increasingly larger than p_0^* as a tissue becomes increasingly unjammed (Fig. 2). This prediction is precisely realized in cultures from primary cells in human patients, with implications for asthma pathobiology[43].

We expect that this rigidity framework will help experimentalists develop other testable hypotheses about how the mechanical response of tissues depends on single-cell properties. For example, Sadati *et al.*[44] have proposed a jamming phase diagram where tissues become more solid-like as adhesion increases, based on observations of jamming in adhesive particulate matter at densities far below confluency. Using standard interpretations of the vertex model (equations (1) and (2)), p_0 increases with increasing adhesion, and therefore our model predicts that confluent tissues become more liquid-like as adhesion increases. This highlights the fact that adhesion acts differently in particulate and confluent materials; in particulate matter higher adhesion leads to gelation and solidification, whereas in the vertex model larger adhesion leads to larger perimeters, more degrees of freedom, and liquid-like behaviour. These ideas suggest that the role of adhesion in tissue rheology may be much richer and more interesting than previously thought.

In addition, although all published vertex models assume three-fold coordinated vertices, there is no proof that such structures are stable for $p_0 > p_0^{hex}$ (ref. 16). Furthermore, higher-order vertices are apparently stabilized in some anisotropic biological tissues, including rosette formation in Drosophila[45]. It will be interesting to study what conditions stabilize higher-fold vertices.

This work may also be relevant to modelling the epithelial-to-mesenchymal transition (EMT) that occurs during cancer tumorigenesis. During EMT, epithelial cells with well-defined, compact shapes and small perimeters relative to their areas transition to mesenchymal cells with irregular shapes and large perimeters relative to their areas[46]. As equation (2) specifies a fixed shape index, one could interpret EMT as an increase in p_0 leading to a solid-to-liquid transition, providing a simple mechanical explanation for the role EMT plays in metastasis. To explore this idea further, it will be necessary to determine if a similar rigidity transition exists in three dimensions. A simple extension of this model would replace perimeters and areas in equation (2) with surface areas and volumes, respectively; this is a promising avenue for future work.

We expect that this model may be of interest to scientists independent of its biological relevance. We have shown it exhibits a simple rigidity transition with a novel control parameter, and therefore it might provide a useful bridge between jamming transitions in particulate matter[6,40] and rigidity transitions in random elastic networks[35–37]. In particular, the potential grouping of vertices into functional cell units could draw an explicit connection between spring networks and particle/cell packings. An open question is whether our model belongs to an existing universality class, and whether the transition is mean-field.

Finally, the fact that the vertex model exhibits disordered ground states for $p_0 > p_0^*$ suggests that it may be a useful toy model for thermodynamic (as opposed to kinetic) explanations of the glass transition in particulate matter. Furthermore, these states are predicted to be hyperuniform[47] with a photonic bandgap, indicating that they may be useful for designing metamaterials with interesting optical properties.

Methods

Methods and any associated references are available in the online version of the paper.

Received 25 January 2015; accepted 11 August 2015; published online 21 September 2015

References

1. Schoetz, E.-M., Lanio, M., Talbot, J. A. & Manning, M. L. Glassy dynamics in three-dimensional embryonic tissues. *J. R. Soc. Interface* **10,** 20130726 (2013).
2. Angelini, T. E. *et al.* Glass-like dynamics of collective cell migration. *Proc. Natl Acad. Sci. USA* **108,** 4714–4719 (2011).
3. Nnetu, K. D., Knorr, M., Käs, J. & Zink, M. The impact of jamming on boundaries of collectively moving weak-interacting cells. *New J. Phys.* **14,** 115012 (2012).
4. Haxton, T. K., Schmiedeberg, M. & Liu, A. J. Universal jamming phase diagram in the hard-sphere limit. *Phys. Rev. E* **83,** 031503 (2011).
5. Abate, A. R. & Durian, D. J. Topological persistence and dynamical heterogeneities near jamming. *Phys. Rev. E* **76,** 021306 (2007).
6. Liu, A. J. & Nagel, S. R. The jamming transition and the marginally jammed solid. *Annu. Rev. Condens. Matter Phys.* **1,** 347–369 (2010).
7. Vicsek, T., Czirók, A., Ben-Jacob, E., Cohen, I. & Shochet, O. Novel type of phase transition in a system of self-driven particles. *Phys. Rev. Lett.* **75,** 1226–1229 (1995).
8. Henkes, S., Fily, Y. & Marchetti, M. C. Active jamming: Self-propelled soft particles at high density. *Phys. Rev. E* **84,** 040301 (2011).
9. Chate, H., Ginelli, F., Gregoire, G., Peruani, F. & Raynaud, F. Modeling collective motion: Variations on the Vicsek model. *Eur. Phys. J. B* **64,** 451–456 (2008).
10. Berthier, L. Nonequilibrium glassy dynamics of self-propelled hard disks. *Phys. Rev. Lett.* **112,** 220602 (2014).
11. Berthier, L. & Kurchan, J. Non-equilibrium glass transitions in driven and active matter. *Nature Phys.* **9,** 310–314 (2013).
12. Petitjean, L. *et al.* Velocity fields in a collectively migrating epithelium. *Biophys. J.* **98,** 1790–1800 (2010).
13. Nagai, T. & Honda, H. A dynamic cell model for the formation of epithelial tissues. *Phil. Mag. B* **81,** 699–719 (2001).
14. Farhadifar, R., Röper, J.-C., Aigouy, B., Eaton, S. & Jülicher, F. The influence of cell mechanics, cell–cell interactions, and proliferation on epithelial packing. *Curr. Biol.* **17,** 2095–2104 (2007).
15. Hufnagel, L., Teleman, A. A., Rouault, H., Cohen, S. M. & Shraiman, B. I. On the mechanism of wing size determination in fly development. *Proc. Natl Acad. Sci. USA* **104,** 3835–3840 (2007).
16. Staple, D. B. *et al.* Mechanics and remodelling of cell packings in epithelia. *Eur. Phys. J. E* **33,** 117–127 (2010).
17. Hilgenfeldt, S., Erisken, S. & Carthew, R. W. Physical modeling of cell geometric order in an epithelial tissue. *Proc. Natl Acad. Sci. USA* **105,** 907–911 (2008).
18. Manning, M. L., Foty, R. A., Steinberg, M. S. & Schoetz, E.-M. Coaction of intercellular adhesion and cortical tension specifies tissue surface tension. *Proc. Natl Acad. Sci. USA* **107,** 12517–12522 (2010).
19. Wang, G., Manning, M. L. & Amack, J. D. Regional cell shape changes control form and function of Kupffer's vesicle in the zebrafish embryo. *Dev. Biol.* **370,** 52–62 (2012).
20. Chiou, K. K., Hufnagel, L. & Shraiman, B. I. Mechanical stress inference for two dimensional cell arrays. *PLoS Comput. Biol.* **8,** e1002512 (2012).
21. Fletcher, A. G., Osterfield, M., Baker, R. E. & Shvartsman, S. Y. Vertex models of epithelial morphogenesis. *Biophys. J.* **106,** 2291–2304 (2014).
22. Hočevar, A. & Ziherl, P. Degenerate polygonal tilings in simple animal tissues. *Phys. Rev. E* **80,** 011904 (2009).
23. Zehnder, S. M., Suaris, M., Bellaire, M. M. & Angelini, T. E. Cell volume fluctuations in MDCK monolayers. *Biophys. J.* **108,** 247–250 (2015).
24. Graner, F. & Glazier, J. A. Simulation of biological cell sorting using a two-dimensional extended Potts model. *Phys. Rev. Lett.* **69,** 2013–2016 (1992).
25. Amack, J. D. & Manning, M. L. Extending the differential adhesion hypothesis in embryonic cell sorting. *Science* **338,** 212–215 (2012).
26. Lecuit, T. "Developmental mechanics": Cellular patterns controlled by adhesion, cortical tension and cell division. *HFSP J.* **2,** 72–78 (2008).
27. Guillot, C. & Lecuit, T. Mechanics of epithelial tissue homeostasis and morphogenesis. *Science* **340,** 1185–1189 (2013).
28. Weaire, D. L. & Hutzler, S. *The Physics of Foams* (Oxford Univ. Press, 1999).
29. Bi, D., Lopez, J. H., Schwarz, J. M. & Manning, M. L. Energy barriers and cell migration in densely packed tissues. *Soft Matter* **10,** 1885–1890 (2014).
30. Newhall, K. A., Jorjadze, I., Vanden-Eijnden, E. & Brujic, J. A statistical mechanics framework captures the packing of monodisperse particles. *Soft Matter* **7,** 11518–11525 (2011).
31. Aste, T. & Di Matteo, T. Emergence of gamma distributions in granular materials and packing models. *Phys. Rev. E* **77,** 021309 (2008).
32. Bi, D., Zhang, J., Behringer, R. P. & Chakraborty, B. Fluctuations in shear-jammed states: A statistical ensemble approach. *Europhys. Lett.* **102,** 34002 (2013).
33. Kadanoff, L. P. *et al.* Static phenomena near critical points: Theory and experiment. *Rev. Mod. Phys.* **39,** 395–431 (1967).
34. Olsson, P. & Teitel, S. Critical scaling of shear viscosity at the jamming transition. *Phys. Rev. Lett.* **99,** 178001 (2007).
35. Das, M., Quint, D. A. & Schwarz, J. M. Redundancy and cooperativity in the mechanics of compositely crosslinked filamentous networks. *PLoS ONE* **7,** e35939 (2012).
36. Broedersz, C. P., Mao, X., Lubensky, T. C. & MacKintosh, F. C. Criticality and isostaticity in fibre networks. *Nature Phys.* **7,** 983–988 (2011).
37. Heussinger, C. & Frey, E. Floppy modes and nonaffine deformations in random fiber networks. *Phys. Rev. Lett.* **97,** 105501 (2006).
38. Ashcroft, N. W. & Mermin, N. D. *Solid State Physics* HRW International edn (Holt, Rinehart and Winston, 1976).
39. Silbert, L. E., Liu, A. J. & Nagel, S. R. Vibrations and diverging length scales near the unjamming transition. *Phys. Rev. Lett.* **95,** 098301 (2005).
40. Wyart, M., Silbert, L. E., Nagel, S. R. & Witten, T. A. Effects of compression on the vibrational modes of marginally jammed solids. *Phys. Rev. E* **72,** 051306 (2005).
41. Manning, M. L. & Liu, A. J. A random matrix definition of the boson peak. *Europhys. Lett.* **109,** 36002 (2013).
42. O'Hern, C. S., Langer, S. A., Liu, A. J. & Nagel, S. R. Random packings of frictionless particles. *Phys. Rev. Lett.* **88,** 075507 (2002).
43. Park, J.-A. *et al.* Unjamming and cell shape in the asthmatic airway epithelium. *Nature Mater.* http://dx.doi.org/63x (2015).
44. Sadati, M., Qazvini, N. T., Krishnan, R., Park, C. Y. & Fredberg, J. J. Collective migration and cell jamming. *Differentiation* **86,** 121–125 (2013).
45. Kasza, K. E., Farrell, D. L. & Zallen, J. A. Spatiotemporal control of epithelial remodeling by regulated myosin phosphorylation. *Proc. Natl Acad. Sci. USA* **111,** 11732–11737 (2014).

46. Kalluri, R., Weinberg, R. A. *et al.* The basics of epithelial–mesenchymal transition. *J. Clin. Invest.* **119,** 1420–1428 (2009).
47. Gabrielli, A. & Torquato, S. Voronoi and void statistics for superhomogeneous point processes. *Phys. Rev. E* **70,** 041105 (2004).

Acknowledgements

We would like to thank G. Salbreux and M. C. Marchetti for substantial and useful comments on this manuscript. M.L.M. acknowledges support from the Alfred P. Sloan Foundation, and M.L.M. and D.B. acknowledge support from NSF-CMMI-1334611 and NSF-DMR-1352184. M.L.M. and D.B. also would like to thank the KITP at the University of California Santa Barbara for hospitality, supported in part by NSF PHY11-25915. The authors also acknowledge the Syracuse University HTC Campus Grid and NSF award ACI-1341006.

Author contributions

D.B., M.L.M. and J.M.S. conceived and designed the project, which was executed and analysed by D.B. and J.H.L., with oversight from J.M.S. and M.L.M. D.B., J.M.S. and M.L.M. prepared the manuscript.

Additional information

Supplementary information is available in the online version of the paper. Reprints and permissions information is available online at www.nature.com/reprints. Correspondence and requests for materials should be addressed to M.L.M.

Competing financial interests

The authors declare no competing financial interests.

Methods

Simulating a confluent tissue monolayer. To simulate confluent monolayers, a random sequential addition point pattern[48] of M points was generated under periodic boundary conditions, with box size L chosen such that the average area per cell is unity. Two methods of generating this initial point pattern were used: a random sequential addition point pattern[48], and a Poisson point pattern. The results presented in this work are independent of the method of initial point pattern generation. A Voronoi tessellation of this point pattern results in a disordered cellular structure, which was then used as an input to the program Surface Evolver[49]. Surface Evolver numerically minimizes the total energy of the system (equation (2)) at fixed topology using gradient descent with respect to the vertices of the cells. If an edge shrinks below a threshold value l^*, a passive T1 transition is allowed if it lowers the energy. On the solid side of the transition, all structures are minimized such that the average energy of a cell changes by less than one part in 10^{10} between consecutive minimization steps, and as in other simulations of the vertex model[15,16]. On the fluid side of the transition, minimization is challenging given the flat nature of the landscape, for the same reasons the shear modulus is difficult to calculate near the transition, as discussed in more detail in Supplementary Section III. Therefore, if the algorithm does not reach the energy change threshold, the minimization algorithm is stopped after 500,000 minimization steps.

Once an initial energy-minimized state is reached, T1 transitions are actively induced at every edge to measure energy barriers[29]. An example of a T1 in the simple four-cell case is shown in Fig. 1a: the central thick edge is quasi-statically contracted to zero length ($\ell = 0$), at which point a T1 topological swap is executed. After the T1, the length of the central edge is then expanded until it reaches the initial length ($\ell = \ell_0$). The total energy of four cells during this process is shown in Fig. 5b; the edge length is represented by a negative value during contraction and flips sign after the T1.

For each active T1 transition in an N-cell system, the energy barrier is defined as the total energy difference between the initial state $\ell = \ell_0$ and the onset of T1 topological swap ($\ell = 0$). Calculations of energy barriers were repeated for various values of r at decadal increments from 0.005 to 200 and p_0 ranging from 3 to 4.

To calculate the shear modulus, we apply quasistatic simple shear to a tissue using Lees–Edwards periodic boundary conditions. The shear modulus is calculated by taking the linear response of the tissue, as defined by equation (6):

$$G_{xy} = \frac{1}{L^2} \lim_{\gamma_{xy} \to 0} \frac{\partial^2 \varepsilon}{\partial \gamma_{xy}^2} \tag{6}$$

where L is the linear dimension of the tissue.

Calculation of the vibration density of states. We obtain the vibrational density of states by diagonalizing the Hessian matrix of the system

$$H_{i\mu j\nu} = \frac{\partial^2 \varepsilon}{\partial r_{i\mu} r_{j\nu}} \tag{7}$$

where i,j are indices for vertices and μ,ν Cartesian coordinates, and ε is defined in equation (2). The eigenvalues of equation (7) are $\{\lambda_i\}$.

All of these eigenvalues should be positive or zero for a minimized system. On the fluid side of the transition, where the minimization is challenging because the landscape is completely flat, this algorithm finds negative eigenvalues that are very close to zero (10^{-4} of the average positive eigenvalue). Therefore, we label these very small negative eigenvalues as zero to within our numerical precision, and they are included in $N(\lambda = 0)$ through the manuscript.

References

48. Torquato, S. & Haslach, H. W. Jr Random heterogeneous materials: Microstructure and macroscopic properties. *Appl. Mech. Rev.* **55,** B62–B63 (2002).
49. Brakke, K. A. The Surface Evolver. *Exp. Math.* **1,** 141–165 (1992).